AD-A034 410 MATERIALS RESEARCH LABS MARIBYRNONG (AUSTRALIA) F/G 11/2
INTERACTION OF PULSED CO2-LASER RADIATION WITH NON-METALS,(U)
JUN 76 D R BRIGHTON, W E GIBBS
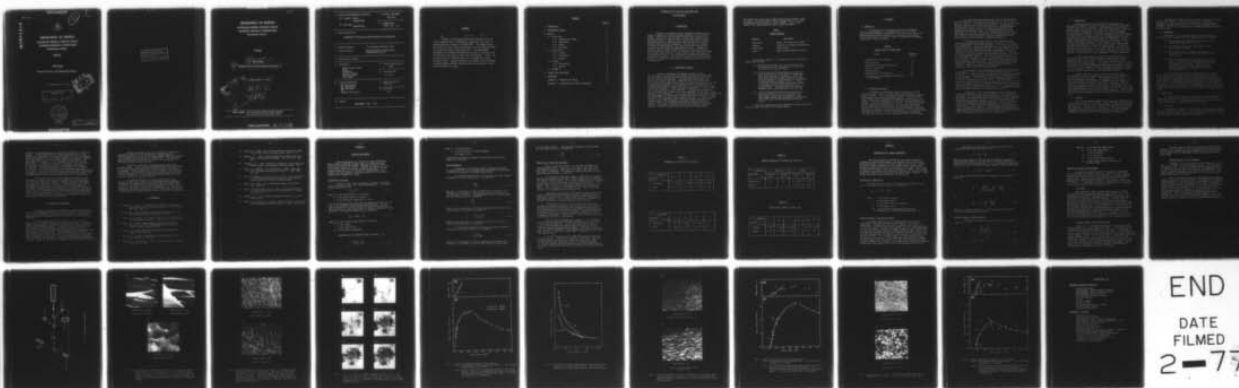
UNCLASSIFIED MRL-R-663 NL

| OF |
AD
A034410

END
DATE
FILMED
2-77

MRL-R-663

AR-273

ADA034410

DEPARTMENT OF DEFENCE

AUSTRALIAN DEFENCE SCIENTIFIC SERVICE

MATERIALS RESEARCH LABORATORIES

MARIBYRNONG VICTORIA

REPORT

MRL-R-663

INTERACTION OF PULSED CO_2-LASER RADIATION WITH NON-METALS

D. R. Brighton and W. E. K. Gibbs

D D C

JAN 14 1977

APPROVED

FOR PUBLIC RELEASE

MELBOURNE

JUNE 1976

AR-273

DEPARTMENT OF DEFENCE

AUSTRALIAN DEFENCE SCIENTIFIC SERVICE

MATERIALS RESEARCH LABORATORIES

MARIBYRNONG VICTORIA

REPORT

MRL-R-663

INTERACTION OF PULSED CO_2-LASER RADIATION WITH NON-METALS

D. R. Brighton and W. E. K. Gibbs

Jun 76

37p.

POSTAL ADDRESS: Chief Superintendent, Materials Research Laboratories, P.O. Box 50, Ascot Vale, Victoria 3032, Australia

1. Security Grading/Release Limitation

    (a) Document content:

                UNCLASSIFIED

    (b) This page:

                UNCLASSIFIED

2. Document Type/Number

          MRL-R-663

3. Document Date

          JUNE, 1976

4. Title and Sub-Title

      INTERACTION OF PULSED CO_2-LASER RADIATION WITH NON-METALS

5. Personal Authors: D.R. Brighton and W.E.K. Gibbs

6. Corporate Author: Materials Research Laboratories,
                             Maribyrnong, Victoria

7. Abstract (See reverse)

8. Descriptors

        Carbon Dioxide Lasers
        Damage
        Non-Metals
        Specific Impulse
        Detonation Waves
        Laser Beams

9. Cosati Classifications

          20-05

11. Task Reference

          DST 63/03

10. Library distribution

    MRL (Maribyrnong)
    MRL (NSW Branch)
    MRL (SA Branch)
    WRE
    Campbell Park Library

12. Sponsoring Agency
      Reference

13. Cost Code

          41740

14. Imprint

        MARIBYRNONG - MRL - 1976

ABSTRACT

Samples of crown glass, fused silica, Perspex and Irtran 1 were irradiated with 0.2-μs duration pulses from a CO_2 laser, at energy densities of between 10 and 800 kJ/m^2. The damage induced was thermal in origin and was controlled more by the absorption depth in the material than by thermal diffusion. The major damage mechanisms were cracking and flaking in the case of crown glass, and vaporisation in the cases of fused silica and Perspex. Irtran 1 was the most difficult to damage because of its comparatively large absorption depth. Impulse production was studied, and was explained by simple models involving vaporisation and the excitation of laser-supported detonation waves.

ii

CONTENTS

INTERACTION OF PULSED CO$_2$-LASER RADIATION

WITH NON-METALS

1. INTRODUCTION

There is a considerable body of literature dealing with the effects on materials of pulsed CO$_2$-laser radiation at 10.6- μm wavelength. Much of this work has been concerned with studies of the plasmas produced near metal surfaces by pulses with durations in the microsecond region. However, studies of the interaction of pulses with durations in the submicrosecond region with metals[1,2] and non-metals[3,4] have not been as extensive. The purpose of this paper is to extend the understanding of the damage mechanisms involved when non-metals are irradiated by submicrosecond pulses. Although the materials studied (crown glass, fused silica, Perspex and Irtran 1) are all strong absorbers of 10.6- μm radiation, their absorption depths are somewhat larger than the thermal diffusion depth corresponding to a submicrosecond pulse. This represents a situation different from that usually discussed[5,10] in which the deposition of energy within the material is assumed to be controlled by thermal diffusion rather than by absorption.

2. EXPERIMENTAL DETAILS

The basic experimental arrangement is shown in Fig. 1. The laser used in this work utilised pulsed electron-beam preionisation derived from two cold-cathode electron guns, but for most of the work only one electron gun was used. When operated in this manner, the laser gave an output pulse which consisted of an initial spike about 0.2 μs wide at half height, followed by a much smaller peak with a 2-μs tail. Although higher energies could be achieved by the use of both guns, the resulting pulse shape was erratic and only a small amount of work was done under these conditions. Pulse waveforms were monitored by a photon-drag detector and displayed on an oscilloscope. Energies were measured by a disc calorimeter with a readout unit that compensated for the thermal time-constant of the calorimeter. The focusing lens had a focal length of 370 mm and the energy density on the sample could be varied between 10 kJ/m^2 (1 J/cm^2) and 800 kJ/m^2 by varying the lens-to-sample distance. In addition, small changes to the energy were made by inserting polyethylene films in the unfocused beam. The irradiated areas, which could be varied from 30 mm^2 to 400 mm^2, were determined from the burn patterns produced in Perspex. Variations of irradiation within the irradiated area were neglected and thus the energy densities quoted are average values.

The samples were in the form of small discs and were mounted so that the angle of incidence could be varied, although most of the results reported here were obtained at normal incidence.   Table 1 gives details of the sample materials used in these experiments.

TABLE 1

SAMPLE MATERIALS

MATERIAL	DESCRIPTION
Crown glass	Chance, hard crown, Type 519604
Perspex	Commercial poly(methyl methacrylate)
Fused silica	Optical grade
Irtran 1	Kodak sintered magnesium fluoride

The temporal behaviour of the sample surface was observed in several different ways:

(a)   Photographs were taken at 64 and at 400 frames per second in the case of crown glass, and at 64 frames per second in the case of Irtran 1.

(b)   For both glass and Perspex samples, the beam from a He-Ne laser (see Fig. 1) was directed through the area of the sample to be irradiated.   This probe-laser beam then passed through a pin-hole and was incident adjacent to another pin-hole at the entrance to a photomultiplier as shown in Fig. 1.   Thus, scattering of the probe-laser beam caused by damage to the sample surface could be detected by the photomultiplier.   The photomultiplier signal was displayed on an oscilloscope and a chart recorder.

(c)   The photon-drag detector was used to measure the specular reflection at 10.6-μm wavelength from a glass sample, for an angle of incidence of 45$^{\text{O}}$. The incident waveform was monitored by a pyroelectric detector in place of the photon-drag detector in Fig. 1.

A ballistic pendulum was used to measure the impulse imparted to the crown glass, fused silica and Perspex samples.

3. RESULTS

3.1 CROWN GLASS

The morphology of the damaged surfaces was examined by an optical microscope and a scanning electron microscope (SEM). Many different phenomena were observed in the glass itself and in the plasma resulting from the interaction of the beam with the sample. Some of these effects are listed in Table 2 together with approximate thresholds for their occurrence.

TABLE 2

DAMAGE EFFECTS IN CROWN GLASS

EFFECT	THRESHOLD (kJ/m^2)
Perpendicular crack formation	5
Flake formation	10
Vaporisation and impulse production	20
Uniform "orange-peel"	40
Fringe patterns	60
Disappearance of "orange-peel"	100
Peak impulse and laser-supported detonation-wave formation	250

3.1.1 Cracking and Flaking

Micrographs of the damaged samples showed that at energy densities around 5 kJ/m^2, localised cracking perpendicular to the surface occurred. The cracks usually had multiple branches although long straight cracks were occasionally observed. Above 10 kJ/m^2, flakes formed due to cracking both perpendicular and parallel to the surface. The partial detachment of the flakes from the substrate was apparent in the SEM micrographs (Fig. 2a, b). (This detachment could also be inferred from the presence of circular interference fringes when the samples were viewed in reflected light under the optical microscope). There did not appear to be any intermediate stage where extensive perpendicular cracking only took place. Just above threshold the flakes were regular in shape, often approximately rectangular (see Fig. 2b), but further above threshold the flakes were irregular.

The flake thicknesses were measured from the SEM micrographs of flakes that had curled sufficiently to give a clear view of the edge (e.g. Fig. 2a). The thickness obtained was 5 ± 2 µm, with little apparent variation with incident energy density. Thicknesses were also measured using the optical microscope by the standard method of focusing on the surface, then on the flake-substrate junction and correcting for refractive index. The thickness obtained by this method was 7.5 ± 2.5 µm. There was a large variation in the size of the flakes formed, but the majority were in the range from 40 µm to 300 µm across. The average flake area was approximately 0.01 mm^2 but areas did differ by an order of magnitude either way.

The photographic observations of the irradiated surface showed that cracking and flaking proceeded in two main stages that were distinguished by their time dependence. Initially, a fast stage was apparent where a relatively small number of long cracks divided the irradiated area into independent regions. This was followed by a slow stage in which these regions either broke into flakes or were criss-crossed by another set of cracks before flaking occurred. (Fig. 3a is an optical micrograph showing two long cracks and some of the flakes in three independent regions). The initial cracks took less than 2.5 ms to form and a typical region took approximately 30 ms to break up into flakes. However, some regions did not commence breaking up until 100 ms after the laser pulse. The regions that broke up first formed flakes that were larger than those from the regions that broke up later. Figure 4 is a series of 6 frames, taken 15 ms apart, illustrating the cracking and flaking processes.

An analysis of the cracking and flaking processes is presented in Appendix 1. In this analysis, absorption rather than thermal diffusion[6,7] is assumed to control the depth at which energy is deposited in the material. This assumption is made since, in this material, the absorption depth ($\simeq 1$ µm)[8] is larger than the thermal diffusion depth ($\simeq 0.6$ µm) corresponding to a 0.2-µs pulse. The energy density required to soften the glass surface is calculated to be about 2.2 kJ/m^2 and it is estimated that on cooling the tensile stress developed would exceed the tensile strength of the glass. In view of the assumptions made in the analysis, the above energy density is in reasonable agreement with the observed threshold for cracking of about 5 kJ/m^2.

A comparison of the relative speeds at which cracking and flaking are expected to occur can be obtained from the calculations in Appendix 1 of the elastic energy released per unit surface area in each case. The results show that, in the case of cracking, the energy released greatly exceeds the value of 10 J/m^2 which is required[6] for rapid crack propagation; whereas in the case of flaking the energy released is considerably less than this value. Thus cracking perpendicular to the surface would be expected to proceed at a much faster rate than would flaking. The photographic observations are in general agreement with these predictions in that cracking occurred at speeds greater than those that could be resolved by the camera (10 m/s) and was then followed by flaking at a much slower speed.

3.1.2 Vaporisation

At energy densities around 20 kJ/m^2 vaporisation of the glass surface commenced, imparting an impulse to the sample and forming a bright plasma above the surface. Small undulations in the sample surface, giving it an "orange-peel" appearance, were evident in both the SEM and optical micrographs. (Fig. 3(a) is an optical micrograph illustrating the "orange-peel" overlaying the cracking and flaking). At energy densities of about 40 kJ/m^2 the "orange-peel" is fairly uniform over nearly all of the damaged region but at energy densities of about 60 kJ/m^2 small regions lose their "orange-peel" appearance. These regions often exhibit fringe patterns (see Fig. 3) which are circular for normal incidence and elliptical for other angles of incidence. The patterns are probably the result of interference between the incident radiation and radiation scattered from a point source. Walters[9] has observed similar patterns on acrylic plastic and silica and postulates that the scattering sites act as initiation points for laser-supported detonation (LSD) waves which in turn result in shielding of part of the surface. At about 100 kJ/m^2 the "orange-peel" has almost disappeared.

As only a small amount of material was vaporised from the surface by each pulse, the depth removed by a series of 50 pulses was measured by means of the optical microscope and the average amount removed per pulse was calculated. The results are shown in Fig. 5(a) as a function of energy density. The analysis of vaporisation presented in Appendix 2 shows that agreement with the observed threshold (estimated from Fig. 5(b)) is obtained if material parameters appropriate to fused silica are assumed. However, the amount of material removed at energy densities above threshold could not be predicted accurately.

A He-Ne laser (Fig. 1) was used to investigate the time development of the surface damage, particularly at times shorter than could be resolved by the camera. The scattering from the sample surface developed in two stages: a fast stage and a slow stage. The fast stage presumably corresponded to scattering from the irregular surface left after vaporisation; this type of scattering could be clearly detected 100 µs after the laser pulse. Scattering at earlier times was obscured by the tail of the pulse from the plasma flash. The slow stage presumably corresponded to scattering from the flakes and this took between 0.2 s and 0.8 s to reach its full amplitude. These results are thus in general agreement with the photographic observations reported above.

3.1.3 Impulse

The specific impulse (impulse per unit incident energy) versus energy density is shown in Fig. 5(b). Below 250 kJ/m^2 only one electron gun was used to excite the laser, whereas above 250 kJ/m^2 both electron guns were used. Because of the variable laser-beam pulse waveform the measurements are less reliable in this region. The specific impulse increases as the energy density increases up to 150 kJ/m^2, remains essentially constant until 250 kJ/m^2 and decreases thereafter.

The analysis of impulse production given in Appendix 2 is based on that of Schriempf[10]. Once again, assuming that the material parameters[11] of fused silica are appropriate in this case, reasonable theoretical agreement with the shape of the specific impulse curve is obtained. However, the maximum impulse observed was somewhat less than that calculated.

3.1.1 Reflectance

Measurement of the specular reflectance from the sample, in the energy density range 20-200 kJ/m^2, indicated four main features:

(a) The reflected pulse amplitude became smaller as the energy density increased (see Fig. 6).

(b) The reflected pulse width became smaller as the energy density increased.

(c) As the energy density increased, the peak of the reflected pulse occurred earlier than the peak of the incident pulse.

(d) When two successive pulses were incident on the same area of the sample, it was found that, above a pulse energy of about 100 kJ/m^2, the specular reflectance was the same for each pulse. However, below 100 kJ/m^2 the specular reflectance for the second pulse was somewhat less than that for the first pulse (see Fig. 6).

It is expected that specular reflectance will be determined by the absorption and scattering of the incident and reflected beams in the plasma above the target surface, by the absorption at the target surface and by any additional scattering introduced by the damage to the target surface. The observations are consistent with the interpretation that close to the vaporisation threshold the plasma above the target is transparent to 10.6-μm radiation and the reflectance is mainly determined by the state of the target surface. At higher energy densities the plasma becomes more absorbing and the later part of the pulse is absorbed in the plasma.

3.2 FUSED SILICA

The fused silica samples were subjected, at normal incidence, to pulses with energy densities between 45 kJ/m^2 and 450 kJ/m^2 mostly with a beam area of 40 mm^2. Impulse measurements were made and the morphology of the damaged surfaces was examined by optical microscopy.

3.2.1 Cracking

No cracking or flaking was observed with the fused silica samples, in clear contrast to crown glass. From the analysis in Appendix 1 together with the data from Shand[13], it is clear that the tensile stress on cooling does not exceed the tensile strength of the material.

3.2.2 Vaporisation

Vaporisation commenced at an energy density of about 60 kJ/m^2 imparting an impulse to the sample and forming a plasma above the surface.   At energy densities just above this threshold the surface had a rough appearance when viewed by transmitted light under an optical microscope.   At energy densities of about 120 kJ/m^2 fringe patterns, similar to those discussed in section 3.1.2, were observed and the number of fringe patterns increased with increasing energy density. At energy densities of about 300 kJ/m^2, the surface was almost entirely covered by a series of overlapping fringe patterns often centred on areas that had apparently been partly shielded from the beam.   Fig. 7(a) is an optical micrograph of a surface after exposure to an energy density of 450 kJ/m^2.   The individual fringe patterns are no longer distinguishable but the uneven surface due to the fringes and the partial shielding is apparent.   After the same area was irradiated by several pulses the surface appeared to have a greater roughness.   This can be seen in Fig. 7(b) which is an optical micrograph of a surface after exposure to five pulses, each giving an average energy density of 450 kJ/m^2.

The approximate depth of material removed from each of a set of samples was measured by means of the optical microscope.   The results are shown in Fig. 8(a) as a function of energy density.   These results are consistent with Chang's[11] data on the latent heat of vaporisation. However, better agreement is obtained with the observed threshold energy density (estimated from Fig. 8(b)) if the absorption depth is assumed to be about 3 μm rather than the previously assumed value[8] of 12 μm (see Appendix 2).

3.2.3 Impulse

The measured specific impulse versus energy density is shown in Fig. 8(b) for a beam size of 40 mm^2.   The impulse has a threshold of about 60 kJ/m^2 and increases with energy density up to about 250 kJ/m^2 and then decreases.   The shape of the specific-impulse curve is in reasonable agreement with the theoretical analysis of Appendix 2 but in general the observed magnitude is somewhat less than that predicted.

3.3 PERSPEX

The Perspex samples were irradiated by pulses with energy densities between 20 kJ/m^2 and 550 kJ/m^2, the direction of the beam being normal to the surface.   The beam area was varied but most of the results were obtained with a beam area of 30 mm^2.   Impulse measurements were made and the morphology of the damaged surfaces was examined by both optical and electron microscopy.

3.3.1 Vaporisation

Vaporisation commenced at an energy density ≃ 40 kJ/m^2, imparting an impulse to the target and forming a plasma above the surface.   Micrographs of the surface (Fig. 9 is a SEM micrograph) showed a honeycomb-like structure in which the holes appear to be due to the ejection of volatile material from beneath the surface.

Near the vaporisation threshold fringe patterns were observed usually around a relatively undamaged central region. The interpretation of these patterns was discussed in section 3.1.2 but it was not ascertained whether the scattering was due to surface contamination or to material embedded in the sample material.

The approximate depth of material vaporised by a pulse was determined by means of the optical microscope and this is shown in Fig. 10(a) as a function of energy density. The data near threshold are not inconsistent with the value of latent heat of vaporisation quoted in the literature[14]. However, the analysis of the threshold energy density in Appendix 2 indicates a value for the absorption depth of about 15 μm rather than the value of 30 μm obtained from direct absorption measurements[15].

The time development of the damage was investigated with the He-Ne laser used as a probe as described in section 2(a) except that the direct beam was incident on the photomultiplier aperture and scattering by the damaged region thus caused a reduction in signal. The photomultiplier signal was observed to decrease by the time the laser pulse reached its peak, and the scattering was complete after about 1 μs. This prompt occurrence of damage demonstrated that vaporisation was the dominant damage mechanism for this material.

3.3.2 Impulse

The measured specific impulse versus energy density is shown in Fig. 10(b) for an irradiated area of 30 mm^2. The impulse has a threshold at an energy density of about 40 kJ/m^2, reaches a *maximum* value at energy densities around 125-150 kJ/m^2 and then decreases for energy densities above 150 kJ/m^2. The analysis in Appendix 2 of impulse production gives good agreement with the shape of the observed specific-impulse curve. However, the maximum impulse produced is only about one-tenth of that expected;   reasons for this discrepancy are discussed in the Appendix.

3.4 IRTRAN 1

The Irtran 1 samples were irradiated by pulses with energy densities between 100 kJ/m^2 and 500 kJ/m^2. The beam was incident normal to the surface and irradiated an area of 30 mm^2.

The severity of the damage produced in the Irtran 1 samples was generally less than that in the crown-glass samples, although some samples failed catastrophically. There was considerable variability from shot to shot and, because of the limited number of samples available, the investigation was not as thorough as those of the other materials.

Optical microscopy was sufficient to reveal the main features of the damage produced. Above 100 kJ/m^2, a fine crazing pattern was observed on the surface with individual segments having dimensions of approximately 5 μm across. This mode of damage is probably related to the bulk properties of the material and is in contrast to another mode of damage that appeared to be related to absorbing centres in the material. The presence of such

centres is not surprising since the material is produced by a sintering process. It was observed that if a centre was within 75 μm of the surface (i.e. comparable to the absorption depth[15] of 150 μm) a surface crack was produced, and in some cases a complete chip broke off, probably due to the stress produced by the rapid heating of the centre. The development and breakaway of a chip sometimes occurred after several laser pulses. A third mode of damage was observed on one sample that had received three pulses of total (i.e. cumulative) energy density of 500 kJ/m^2. Cracking perpendicular to and parallel to the surface took place to give a mosaic appearance with individual pieces about 70 μm across. Finally, after several more pulses the sample disintegrated. Photographic observations showed that many small pieces were ejected from the central part of the surface, presumably the pieces of the mosaic.

Complete disintegration of some samples occurred due to the development of three or four full-depth perpendicular cracks extending across the full width of the samples. However, it must be emphasised that there was considerable variability in the behaviour of the samples. Some samples did not develop cracks that resulted in disintegration. One sample disintegrated after 5 pulses with a total energy density of 1250 kJ/m^2. Another sample disintegrated after 2 pulses of total energy density 300 kJ/m^2, while another more opaque sample disintegrated after a single pulse of energy density 180 kJ/m^2. It is probable, although this has not been demonstrated, that the full-depth perpendicular cracks also originated from the absorbing inhomogeneities.

4. SUMMARY AND CONCLUSIONS

The damage to absorbing non-metals due to submicrosecond pulses of 10.6-μm wavelength radiation was found to be thermal in origin and to arise from the deposition of energy near the surface at a depth that is determined more by the absorption depth in the material than by thermal diffusion.

The main damage mechanism for crown glass consists of the heating of a thin surface layer to the softening temperature, following which a tensile stress is developed on cooling that is proportional to the coefficient of thermal expansion. Cracking and flaking of the surface results where the stress exceeds the tensile strength of the glass. The speed at which cracking took place was observed to be much higher than that at which flakes were formed. This observation was found to be consistent with calculations that showed a large difference in the elastic energy released in the two cases. The flaking threshold for crown glass with 0.2-μs pulses was observed to be about 10 kJ/m^2 and the threshold for localised cracking in the absence of flaking was about one-half of this value.

Cracking and flaking could not be produced in fused silica, presumably because of its low coefficient of thermal expansion. Vaporisation was found to be the main damage mechanism and this occurred above a threshold energy density of about 60 kJ/m^2. The significant damage mechanism for perspex was also found to be vaporisation, the threshold for which was about 40 kJ/m^2.

Irtran 1 was difficult to damage because of its greater absorption depth. Minor cracking and chipping were produced apparently by stress generated by absorption at isolated centres in the bulk of the material. Complete failure due to the propagation of perpendicular cracks through the full depth of the sample occurred on occasions with no obvious threshold. It is probable that these perpendicular cracks were also initiated at absorption centres.

The measured variation of specific impulse with energy density for crown glass, fused silica and Perspex could be adequately explained by the standard theory after making reasonable modifications to allow for the effects of finite absorption depth. However, the magnitude of the impulse could not be predicted reliably. The quantity of material removed due to vaporisation of the above materials was also in agreement with the modified theory, except in the case of crown glass.

5. REFERENCES

1.   Siegrist, M., Adam, B. and Kneubuhl, F.,(1973), "Interaction of TEA-CO$_2$ laser pulses with metals enhanced by liquid layers", Phys. Lett. 42A, 352.

2.   Ready, R.F., (1974), "Impulse produced by the interaction of CO$_2$ TEA laser pulses", Appl. Phys. Lett. <u>25</u>, 558.

3.   Field, J.E. and Zafar, M.A., (1972), "The effect of surface films on laser damage in glasses", J. Phys. D: Appl. Phys. <u>5</u>, 2105.

4.   Smith, J.L., (1974), "Target damage studies with a pulsed CO$_2$ TEA laser facility", US Army Missile Command Redstone Arsenal, Technical Report RR-74-6.

5.   Ready, J.F., (1971), "Effects of high power laser radiation", Academic Press, New York.

6.   Dugdale, R.A., (1965), "Thermal shock by gas discharge", Trans. Brit. Ceramic Soc. <u>64</u>, 287.

7.   Dugdale, R.A. and Ford, S.D., (1967), "Heat-pulse effects on glass", J. Mat. Sci. <u>2</u>, 260.

8. Cleek, G.W., (1966), "The optical constants of some oxide glasses in the strong absorption region", Appl. Optics $\underline{5}$, 771.

9. Walters, C.T., (1974), "Surface scattering at LSD-wave initiation sites on non-metallic materials". Appl. Phys. Lett. $\underline{25}$, 696.

10. Schriempf, J.T., (1974), "Response of materials to laser radiation - a short course", Naval Research Laboratory Report 7728.

11. Chang, D.G., Drummond, J.E. and Hall, R.B., (1970), "High power laser radiation interaction with quartz", J. Appl. Phys. $\underline{41}$, 4851.

12. Hall, R.B., Maher, W.E. and Wei, P.S.P., (1973), "An investigation of laser-supported detonation waves", Air Force Weapons Laboratory Technical Report No. AFWL-TR-73-28.

13. Shand, E.B., (1958), "Glass Engineering Handbook", McGraw Hill Book Company Inc.

14. Clark, J.E. and Jellinek, H.H.G., (1965), "Thermal degradation of poly(methyl methacrylate) in a closed system", J. Polymer Sci. A3, 1171.

15. Beckwith, P.J., (1975), Materials Research Laboratories, private communication.

16. Maher, W.E. and Hall, R.B., (1975), "An interferometric investigation of laser-supported absorption waves", J. Appl. Phys. $\underline{46}$, 761.

APPENDIX 1

CRACKING AND FLAKING

The basic mechanism for cracking and flake formation in glass consists of heating a surface layer to a temperature where viscous flow relieves the transient compressive stress so that a tensile stress appears on cooling. Cracking and flaking can occur if the stress exceeds the tensile strength of the glass. In the flaking process the tip of a crack that is perpendicular to the surface turns and propagates approximately parallel to the surface, leading to the formation of a flake.

Threshold for cracking

Consider a laser pulse of duration t_p incident on a sample with an absorption depth δ, and a thermal diffusivity κ. The pulse energy is absorbed so that

$$E = E_o e^{-\alpha x} \qquad \ldots 1.1$$

where E_o is the energy density at the surface

   E is the energy density at a depth x

   α is the absorption coefficient $(\delta = 1/\alpha)$.

If δ is large compared with $2\sqrt{(\kappa t_p)}$ then the conduction of heat into the interior of the sample during the pulse may be ignored. In this case the threshold for viscous flow may be derived by equating the energy absorbed in a thin surface layer to the energy required to bring the layer to the softening temperature T_s, leading to

$$E_{th} = \delta \rho c (T_s - T_o) \qquad \ldots 1.2$$

where E_{th} is the incident energy density at threshold

   ρ is the density

   c is the specific heat

   T_o is the ambient temperature

Dugdale[6] gives the maximum stress on cooling, σ, as

$$\sigma \simeq \frac{Y \alpha' (T_s - T_o)}{1 - \nu} \qquad \ldots 1.3$$

where Y is Young's modulus

α' is the coefficient of linear expansion

ν is Poisson's ratio

If the stress exceeds the strength of the glass then cracking and flaking will take place.

Crack Propagation

A comparison of the speeds at which cracking and flaking are expected to occur can be obtained from calculations of the decrease in elastic energy density associated with each case.

For cracking perpendicular to the surface, the energy released in forming unit area of new surface, γ_c, is given by[6]

$$\gamma_c = \frac{\Delta U_c}{2\ell d} \qquad \ldots \text{1.4}$$

where ΔU_c is the decrease in elastic energy per unit surface area on cracking, ℓ is the length of crack per unit area of the surface and d is the depth of cracking. The normalised decrease in elastic energy per unit surface area, p, is defined[6] as

$$p \approx \frac{\Delta U_c}{U_o} \qquad \ldots \text{1.5}$$

where U_o is the upper limit of the elastic energy per unit surface area in the absence of cracking and is given by[6]

$$U_o = \frac{(1-\nu) \, a \, \sigma_o^2}{Y} \qquad \ldots \text{1.6}$$

where a is the thickness of the softened layer and the subscript "o" indicates the upper limit of a parameter.

In the case of cracking plus flaking, the energy released in forming unit area of new surface, γ_f, is given by[6]

$$\gamma_f = \frac{\Delta U_f}{2(1 + \ell d)} \qquad \ldots \text{1.7}$$

where ΔU_f is the decrease in elastic energy per unit surface area on flaking, ℓ is the length of crack per unit area of the surface and

d is the flake thickness. The normalised decrease in elastic energy per unit surface area, q, is defined as[6]

$$q = \frac{\Delta U_f}{U_o} \qquad \qquad \dots 1.8$$

Comparison of theory and experiment

Table 1.1 lists the values of the relevant parameters for crown glass and silica. Values of κ, ρ, c, T_s, α' and ν were taken from Shand[13]; values of δ were taken from Cleek[8]; and values of Y were taken from Dugdale[6]. The results of calculations based on these values are given in Tables 1.2 and 1.3.

In the case of crown glass, Table 1.2 shows that the cracking threshold calculated from equation 1.2 gives a result that is somewhat less than the observed value. This is to be expected since the condition, $\delta \gg 2\sqrt{(\kappa t_p)}$, is only approximately satisfied in this material. The maximum stress produced on cooling was calculated from equation 1.3 and Table 1.2 shows that this is considerably greater than the breaking stress. Thus cracking would be expected to occur and this predicted behaviour is in agreement with the observations.

Cracking was not observed in the case of fused silica and the reason for this can be seen in Table 1.2 where the maximum stress, as calculated from equation 1.3, is less than, or at least comparable to, the breaking stress. The low value of the stress is a consequence of the small coefficient of thermal expansion in this material.

The parameters relevant to the processes of cracking and flaking in crown glass are given in Table 1.3, in which a was taken as the absorption depth, d was taken as the average flake thickness and ℓ was estimated from the film records in the case of cracking and from the average flake area in the case of flaking. Equation 1.6 was used to calculate U_o, and p and q were estimated from equations 15 and 12 of Dugdale[6] respectively. The values of γ_c and γ_f were then calculated from equations 1.4 and 1.7 respectively.

For the case of perpendicular cracking $\gamma_c \simeq 110$ J/m^2 which is well above the value of 10 J/m^2 which Dugdale[6] states is necessary for rapid crack propagation. On the other hand, the low value of γ_f ($\simeq 1$ J/m^2) indicates that flaking would be expected to proceed much more slowly than perpendicular cracking. Although the value of γ_f is not strongly dependent on flake size it will increase as the flake size increases. Hence larger flakes might be expected to form faster than smaller flakes.

The film observations are in qualitative agreement with the above predictions. Perpendicular cracking was observed to take place at speeds greater than those that could be resolved by the camera (10 m/s) and was then followed by flaking at a much slower speed. It was also observed that the regions that broke into flakes early in the process formed larger flakes than the regions that broke into flakes later.

TABLE 1.1

PARAMETERS FOR CROWN GLASS AND SILICA

parameter / material	K m^2 s^{-1}	δ m	ρ kg m^{-3}	c J kg^{-1} K^{-1}
crown glass	0.4×10^{-6}	1.0×10^{-6}	2.5×10^{3}	1.2×10^{3}
silica	0.9×10^{-6}	1.2×10^{-5}	2.2×10^{3}	1.2×10^{3}

parameter / material	T_s K	Y Pa	α' K^{-1}	ν
crown glass	1020	7×10^{10}	8.0×10^{-6}	0.20
silica	1950	7×10^{10}	5.5×10^{-7}	0.17

TABLE 1.2

CRACKING THRESHOLDS FOR CROWN GLASS AND SILICA

parameter / material	Threshold		Stress	
	Predicted kJ m^{-2}	Observed kJ m^{-2}	Predicted Pa	Breaking Pa
crown glass	2.2	5.0	5.1×10^{8}	1×10^{8}
silica	-	-	7.7×10^{7}	1×10^{8}

TABLE 1.3

CRACKING AND FLAKING IN CROWN GLASS

parameter / process	a m	ℓ m^{-1}	d m	U_o J m^{-2}	$\Delta U/U_o$	γ J m^{-2}
cracking	1×10^{-6}	1×10^{3}	7.5×10^{-6}	4.0	0.4	1.1×10^{2}
flaking	1×10^{-6}	2×10^{4}	7.5×10^{-6}	4.0	0.5	0.9

APPENDIX 2

VAPORISATION AND IMPULSE PRODUCTION

Once the vaporisation threshold for the sample is exceeded a pressure is exerted on the target - the reaction to the action of the vaporised material in leaving the sample surface in the form of a plasma. The specific impulse (impulse per unit incident energy) increases with increasing energy density until the absorption of the incident beam in the ionised plasma becomes so strong that an LSD wave is formed. Now pressure is exerted on the target by the expansion of the LSD wave against the target. The specific impulse then decreases as the energy density increases. These trends can be seen in the data in Figs. 5b, 8b and 10b.

Threshold for Vaporisation

The energy per unit area at the threshold of vaporisation, E_{th}, for the conditions assumed in Appendix 1, is given by

$$E_{th} = \delta \, \rho \, (L_v + c\Delta T_v) \qquad \qquad \dots\ 2.1$$

where δ is the absorption depth

ρ is the sample density

L_v is the latent heat of vaporisation

c is the specific heat

ΔT_v is the difference between the vaporisation temperature, T_v, and the ambient temperature, T_o.

Specific Impulse - Vaporisation Region

A precise calculation of the specific impulse curve requires a knowledge of the vapour pressure of the sample as a function of temperature. Although such information is available for silica[11], the corresponding information could not be located for a multi-component glass such as crown glass. Instead, the simpler formulation used by Schriempf[10] to calculate the specific impulse for metal targets has been adopted. The Schriempf model assumes that all of the energy is deposited at the surface and that the temperature distribution in the material is controlled by the thermal diffusion. In cases where there is a finite absorption depth the energy is deposited in a finite volume and, provided that the thermal diffusion length during the pulse time is less than the absorption depth, a similar temperature distribution, controlled by the absorption coefficient rather than by the thermal diffusivity of the material, will be set up.

The impulse per unit area, I, is the force per unit area, P, multiplied by the time over which it acts.

$$I = P(t_p - t_b) \qquad \dots 2.2$$

where t_p is the duration of the pulse and t_b represents a threshold which Schriempf equates to the time taken to raise the temperature of the surface to the vaporisation point. If it is assumed that the power density is constant, the impulse at energy density E may be expressed as

$$\bar{I} = Pt_p (1 - E_{th}/E) \qquad \dots 2.3$$

It can then be shown that the specific impulse due to vaporisation is given by[10]

$$\frac{I}{E} \simeq \frac{\sqrt{c\Delta T_v}}{\sqrt{3}\left[L_v + c\Delta T_v\right]} \left[1 - \frac{E_{th}}{E}\right] \qquad \dots 2.4$$

or

$$\frac{I}{E} = K_1 \left[1 - \frac{E_{th}}{E}\right] \qquad \dots 2.4a$$

where E_{th} is given by equation 2.1, and K_1 is the specific impulse constant in the vaporisation region.

Specific Impulse - LSD Wave Region

Schriempf[10] calculates the specific impulse in the LSD wave region as

$$\frac{I}{E} \simeq \frac{R_s^2 \, \rho_o^{2/3}}{2R \, t_p^{1/3} \, E^{2/3}} \qquad \dots 2.5$$

or

$$\frac{I}{E} = K_2 \, E^{-2/3} \qquad \dots 2.5a$$

where R_s is the effective sample radius

R is the laser beam radius

ρ_o is the air density

t_p is the pulse width

E is the incident energy density

K_2 is the specific impulse constant in the LSD wave region

Comparison of Theory and Experiment

The relevant parameters, and their sources, for crown glass, silica and Perspex are shown in Table 2.1. Values of L_v and T_v for crown glass could not be found in the literature. L_v may be estimated from the slope, near threshold, of the ablation depth versus energy density curve. From the rather scattered data of Fig. 5a L_v was estimated to be in the range 10-60 MJ/kg. T_v was taken to be the same as for silica. It should be noted that in predicting E_{th}, uncertainties in L_v are more important than uncertainties in T_v.

Thresholds

The parameters in Table 2.1 were substituted into equation 2.1 to predict the vaporisation thresholds given in Table 2.2. The agreement with the observed vaporisation thresholds is not good. For crown glass the value of L_v estimated from Fig. 5a is much higher than the values of L_v encountered for most materials. However, if L_v is taken to be the same as for silica (viz. 6.0 MJ/kg), the predicted threshold (25 kJ/m^2) is much closer to the observed threshold (20 kJ/m^2). The tabulated values of L_v for silica and Perspex are consistent with the data in Figs. 8(a) and 10(a). As the values for ρ, c and T_v should be reliable, this suggests that the differences between the predictions and the observations are due to values of the absorption depth, δ, used. For silica agreement would be obtained if δ = 3 μm rather than 12 μm. This is a large difference, but as the 10.6-μm wavelength lies on the tail of the Si-O absorption band, absorption data may not be very accurate. For Perspex agreement would be obtained if δ = 15 μm rather than 30 μm.

Specific Impulse - Vaporisation Region

Table 2.2 lists predicted and observed values of the specific impulse constant, K_1, in the vaporisation region. The predicted values are higher than the observed values by a factor of 2 for crown glass, a factor of 3 for silica and a factor of 10 for Perspex. In the case of silica, vapour pressure data[11] was used to make a more accurate calculation of the impulse. However, the result was similar to that obtained from the simpler Schriempf model. It is expected that at least part of the discrepancy between the predicted and the observed values of K_1 would be due to the reduction in the effective pulse duration as the latter part of the pulse is absorbed by the plasma in front of the sample. This is expected to be particularly relevant in the case of Perspex where a comparatively large amount of material is vaporised.

The solid curves in Figs. 5b, 8b and 10b were obtained from equation 2.4 by substitution of the observed values of the threshold and the specific impulse constant, rather than the predicted values. It is apparent that the experimental results are well represented by these curves.

Specific Impulse - LSD Wave Region

Schriempf[10] gives the condition for the formation of an LSD wave as $\ell' < R$ where ℓ' is the absorption length in the plasma and R is the beam radius. The electron density in the laser-induced plasma is expected to be about 10^{24} electrons/m^3 [16], the temperature about 30 000 K [12] and the pressure in the shock wave about 10^6 Pa[16]. For these parameters, the standard expression for the absorption length[5] gives a value that is less than R.

Figs. 5b, 8b and 10b show the experimental data on specific impulse as a function of energy density. The dashed curves have the energy dependence of equation 2.5a and the magnitude has been adjusted to give a good fit to the experimental data. Table 2.2 gives the predicted values (defined by equations 2.5 and 2.5a) and the observed values (derived from the dashed curves) of the specific impulse constant in the LSD wave region, K_2. For crown glass and for silica the agreement between the predicted and observed values is good (within 30%), whereas for Perspex the observed specific impulse constant is a factor of two smaller than the predicted value. Thus the shape and the magnitude, of the specific impulse versus energy density curve in the LSD wave region, can be predicted reasonably well.

TABLE 2.1

PARAMETERS FOR CROWN GLASS, SILICA AND PERSPEX

parameter / material	δ m	ρ kg m^{-3}	L_v MJ kg^{-1}	c J kg^{-1} K^{-1}	T_v K
crown glass	1.0×10^{-6} a	2.5×10^3 c	10 – 60 d	1.2×10^3 c	3.5×10^3 e
silica	1.2×10^{-5} a	2.2×10^3 c	6.0 e	1.2×10^3 c	3.5×10^3 e
Perspex	3.0×10^{-5} b	1.2×10^3	1.4 f	1.4×10^3	670 f

a. Reference 8
b. Reference 15
c. Reference 13
d. This experiment
e. Reference 11
f. Reference 14

TABLE 2.2

VAPORISATION THRESHOLD AND SPECIFIC IMPULSE FOR CROWN GLASS, SILICA AND PERSPEX

parameter / material	Vaporisation Threshold		Specific Impulse Constant			
			Vaporisation Region, K_1		LSD Wave Region, K_2	
	Predicted $kJ\ m^{-2}$	Observed $kJ\ m^{-2}$	Predicted $N\ s\ J^{-1}$	Observed $N\ s\ J^{-1}$	Predicted $N\ s\ J^{-1/3}\ m^{-4/3}$	Observed $N\ s\ J^{-1/3}\ m^{-4/3}$
crown glass	35 – 160	20	1.2×10^{-4}	5.5×10^{-5}	4.0×10^{-4}	5.0×10^{-4}
silica	260	60	1.2×10^{-4}	4.2×10^{-5}	4.0×10^{-4}	3.0×10^{-4}
Perspex	60	40	2.0×10^{-4}	2.0×10^{-5}	2.5×10^{-4}	1.3×10^{-4}
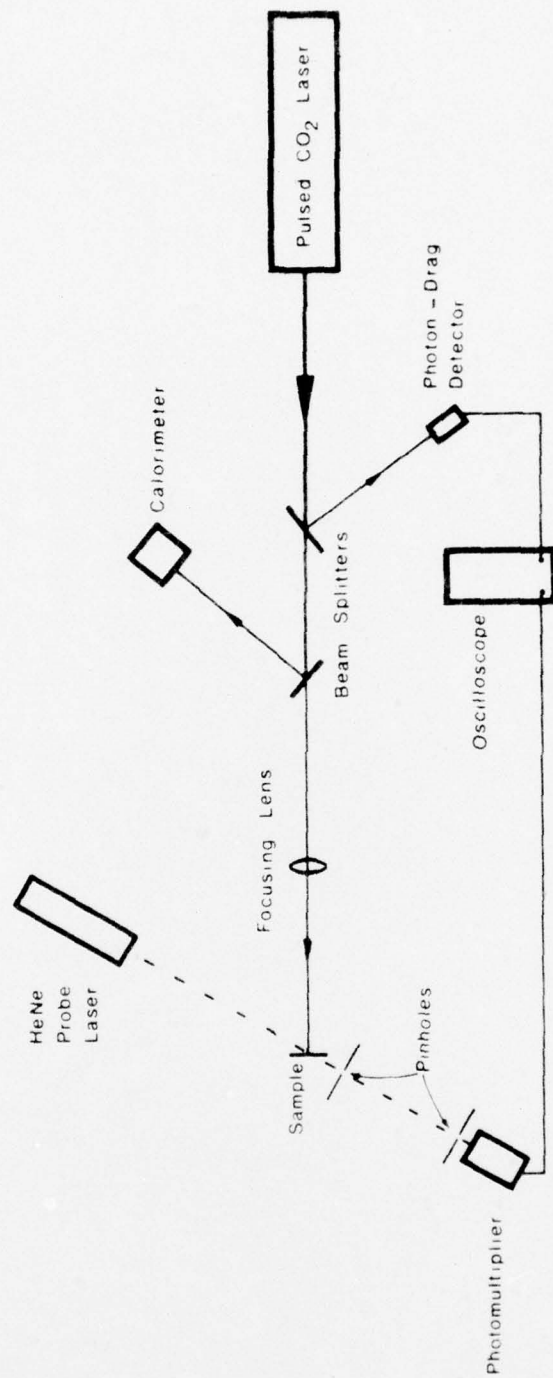
FIG. 1 – Experimental arrangement.

(a)

(b)
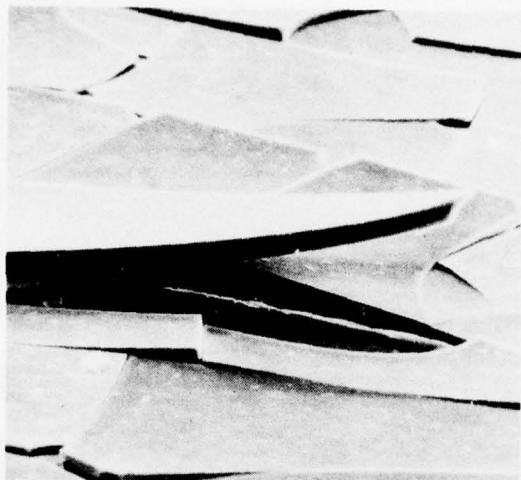
Magnification   X 640

energy density 10kJ/m^2
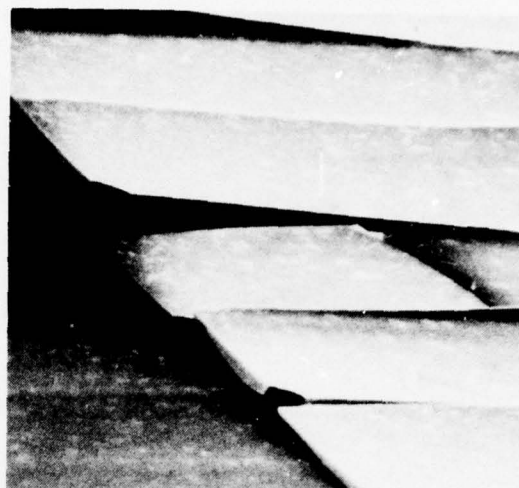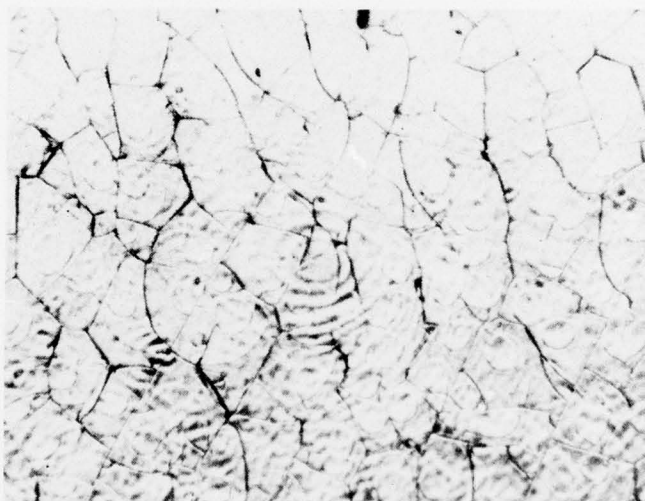

Magnification   X 640

energy density 10kJ/m^2

(c)
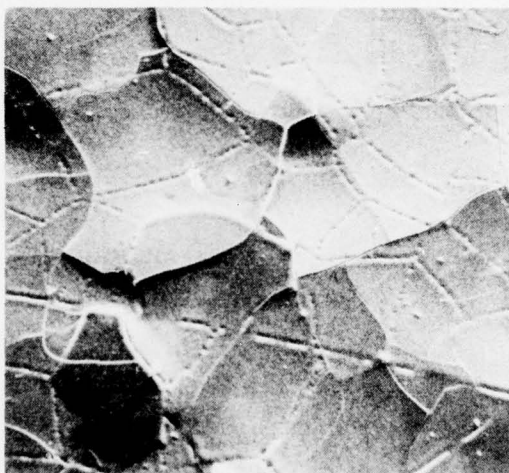
Magnification   X 130

energy density 10KJ/m^2

FIG. 2 – SEM micrographs of damage to crown glass. 2(a) shows a flake that
has lifted away from the substrate. 2(b) shows regular shaped
flakes at the edge of a damaged region. 2(c) was taken after two
pulses were incident on the same area, showing that the first set
of flakes has partly coalesced and that a second set of flakes has
formed.

(a)
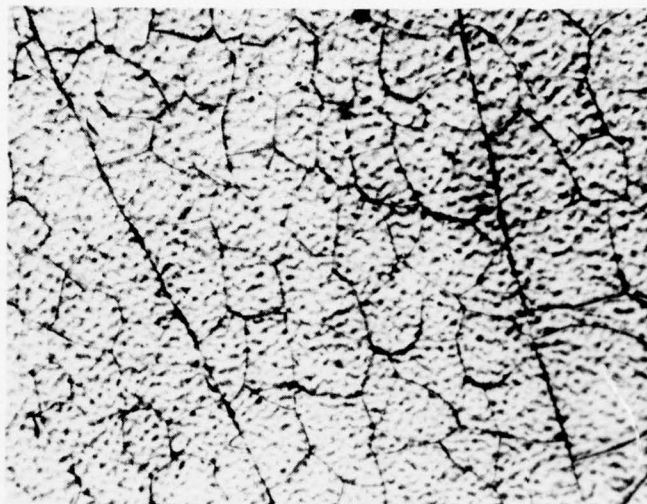
Magnification   X 100

energy density 50 kJ/m^2

(b)

Magnification   X 100

energy density 80 kJ/m^2

FIG. 3 – Optical micrographs of damage to crown glass. 3(a) shows cracking
and flaking overlaid by "orange-peel". Note the two long cracks
that divide the area into three independent regions as far as the
flaking is concerned. 3(b) shows an elliptical fringe pattern
overlaying the flakes.   The beam was incident from the right hand
side at an angle of 45° to the surface.   Note also that there is
very little "orange-peel".

15ms   30ms

45ms   60ms

75ms   90ms

FIG. 4 – Time development of cracking and flaking in crown glass.   The
frames are taken 15ms apart.   Note the long cracks in the early
frames that divide the area into independent regions as far as the
subsequent flaking is concerned.   The energy density was 80 kJ/m^2.
(Magnification X4).
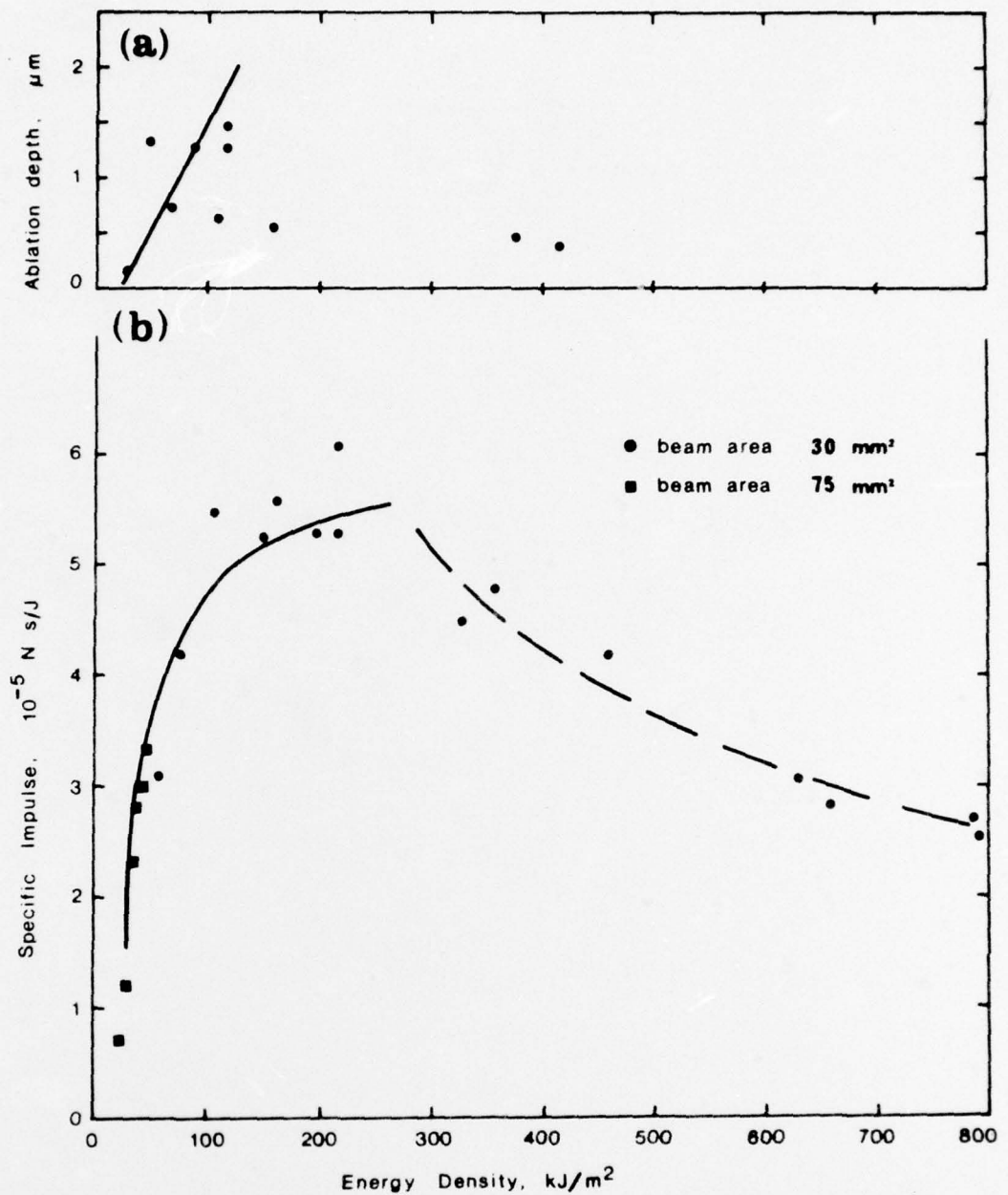
FIG. 5 – Ablation and specific impulse for crown glass.

5(a) – Average ablation depth versus energy density. The straight line represents L_v = 20 MJ/kg.

5(b) – Specific impulse (I/E) versus energy density. The rising portion of the curve corresponds to the vaporisation region and the falling portion to the LSD wave region. The curves are theoretical - see Appendix 2.
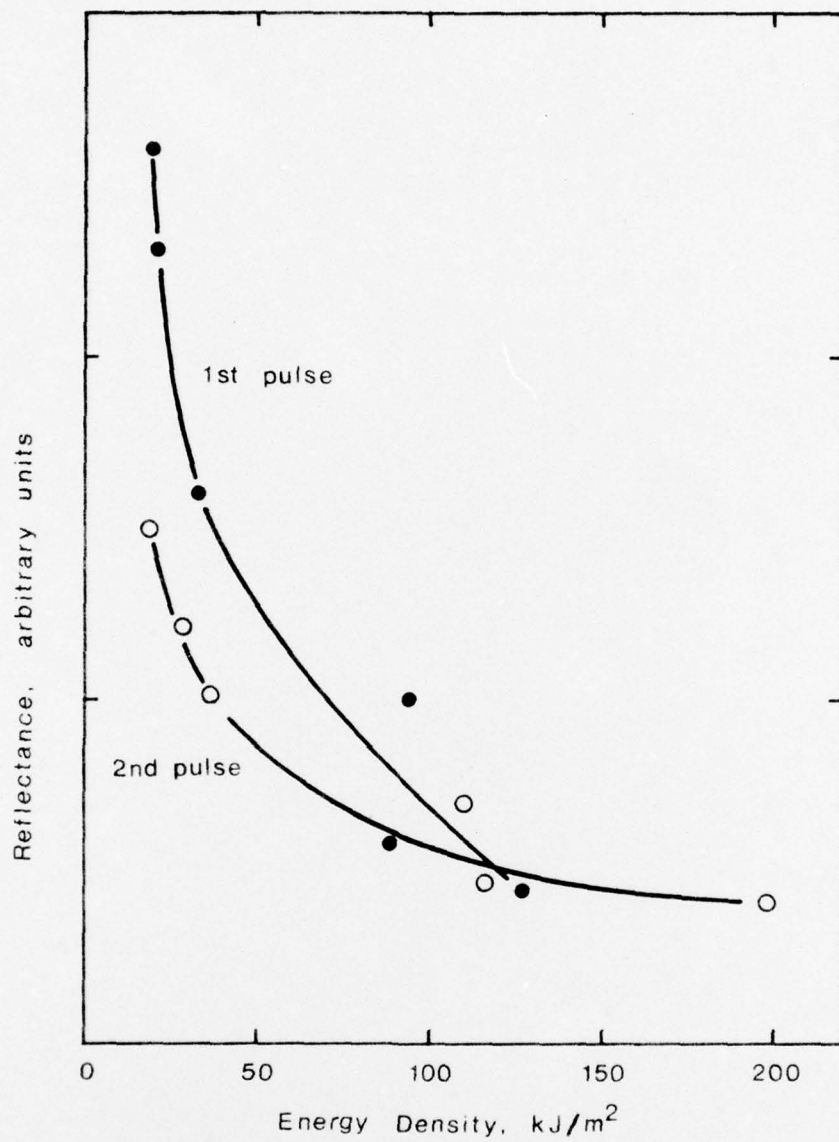
FIG. 6 – Reflectance of 10.6-μm radiation from crown glass after one
and two pulses versus energy density. Reflectance was
measured by the peak voltage from the photon drag detector.

(a)

Magnification X 50

1 pulse, energy density 450 kJ/m^2

(b)
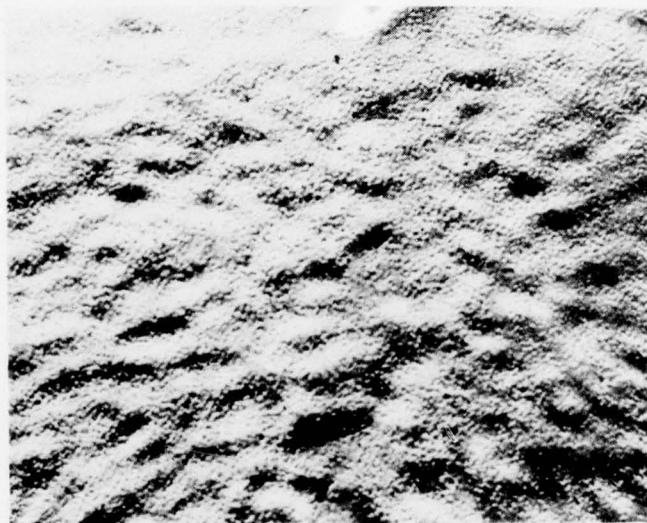
Magnification X 50

5 pulses, average energy density
450 kJ/m^2 each

FIG. 7 - Optical micrographs of damage to fused silica. (a) After a single
        pulse the surface is uneven due to residual fringe patterns and
        partial shielding of certain areas. (b) After 5 pulses the surface
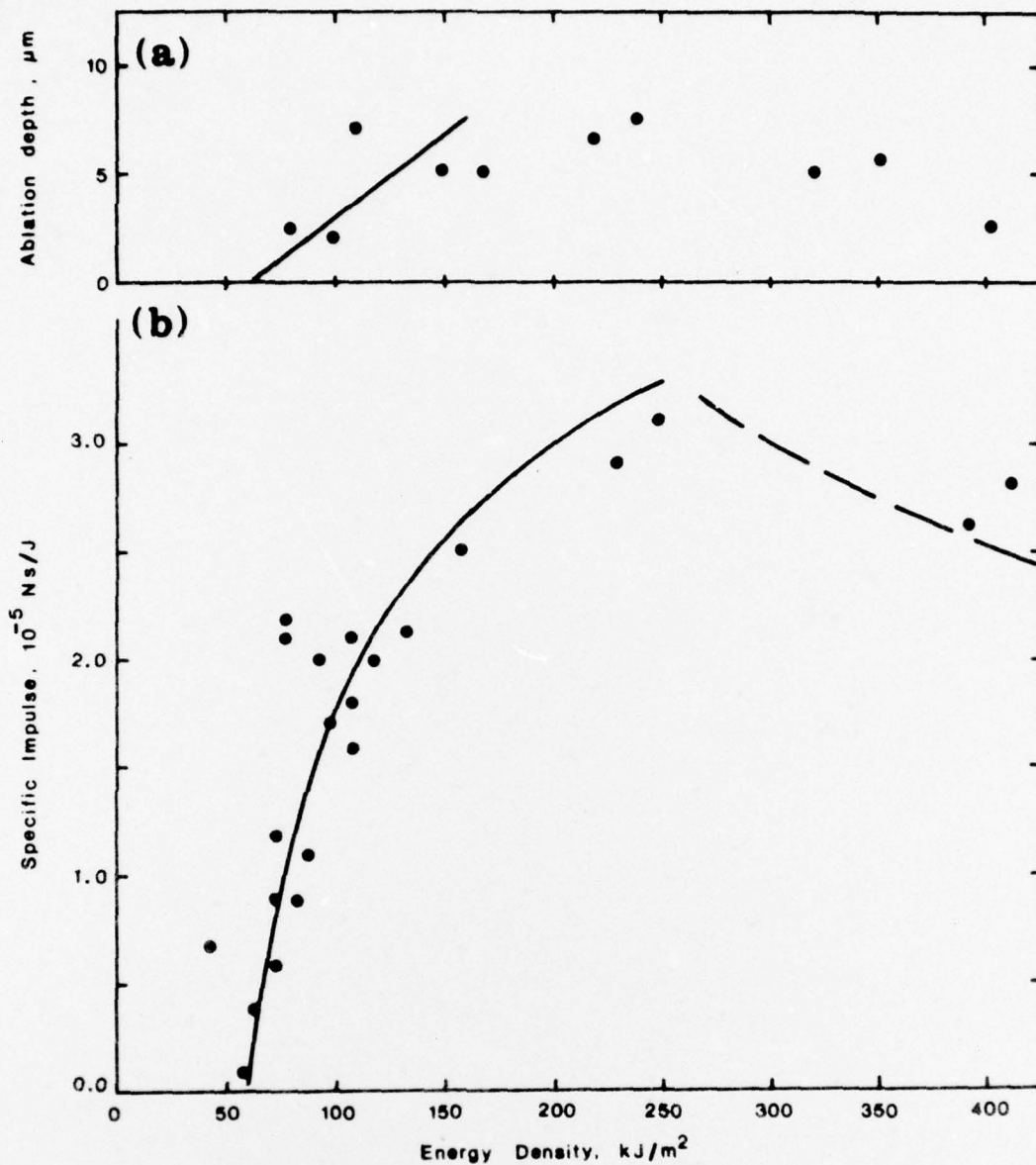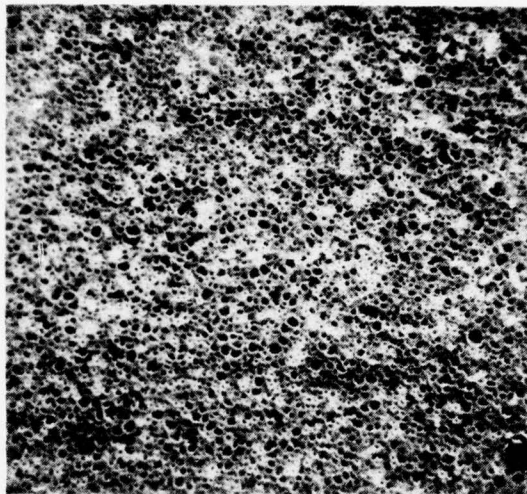   is much rougher.

FIG. 8 – Ablation and specific impulse for fused silica.
   8(a) – Ablation depth versus energy density.   The straight line
      represents $L_v = 6$ MJ/kg.

   8(b) – Specific impulse versus energy density (beam area 40 mm^2).
      The rising portion of the curve corresponds to the
      vaporisation region and the falling portion to the LSD wave
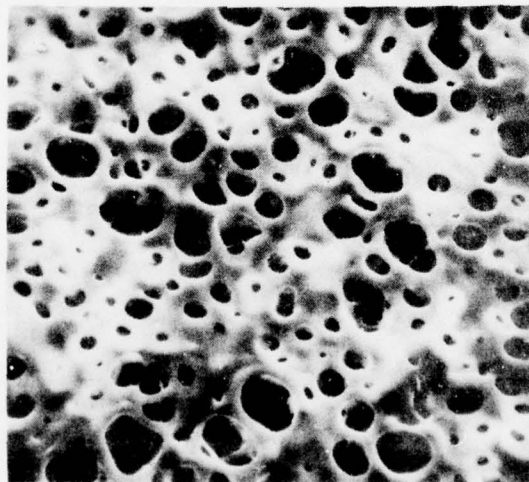   region.   The curves are theoretical – see Appendix 2.

(a)

Magnification   X 112

Energy Density 550 kJ/m^2

(b)

Magnification   X 640

Energy Density 550 kJ/m^2

FIG. 9 – SEM micrographs of damage to Perspex, showing the same sample at
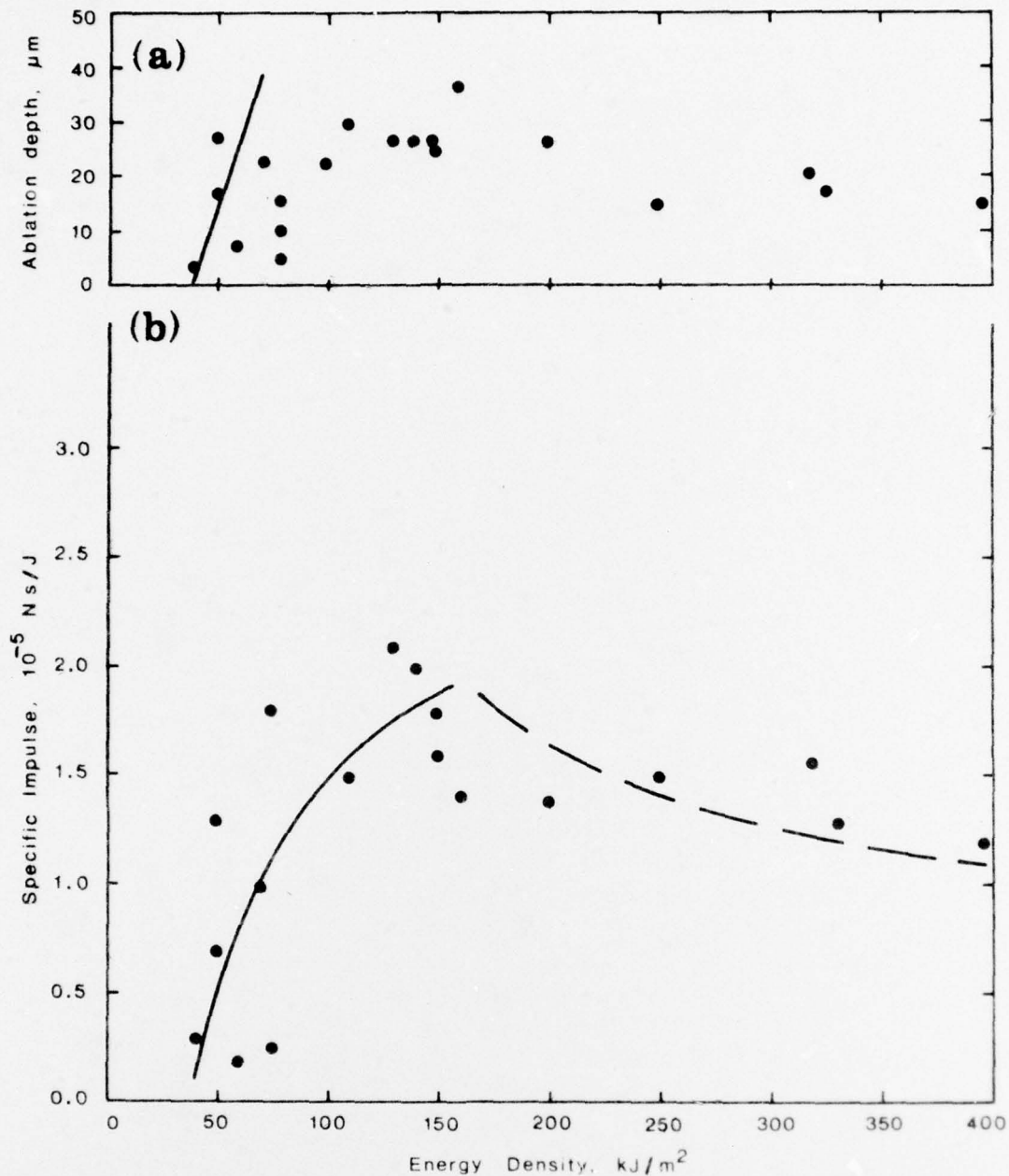different magnifications. Note the honeycomb-like structure.

FIG. 10 - Ablation and specific impulse (I/E) for Perspex.

        10(a) - Ablation depth versus energy density. The straight line represents $L_v = 1.4$ MJ/kg.

        10(b) - Specific impulse versus energy density (beam area 30 mm^2). The rising portion of the curve corresponds to the vaporisation region and the falling portion corresponds to the LSD wave region. The curves are theoretical - see Appendix 2.

DISTRIBUTION LIST

MATERIALS RESEARCH LABORATORIES

Chief Superintendent
Superintendent, Organic Chemistry Division
Superintendent, Physical Chemistry Division
Superintendent, Physics Division
Superintendent, Metallurgy Division
Mr. L.E.S. Mathias
Library
Dr. D.R. Brighton
Mr. W.E.K. Gibbs
Branch Superintendent (S.A. Branch)
Librarian (N.S.W. Branch)
Librarian (S.A. Branch)

DEPARTMENT OF DEFENCE

Chief Defence Scientist
Executive Controller/ADSS
Superintendent, Central Studies Establishment
Superintendent, Defence Science Administration, DSTO
Head, Laboratory Programs Branch
Army Scientific Adviser
Air Force Scientific Adviser
Naval Scientific Adviser
Chief Superintendent, Aeronautical Research Laboratories
Director, Weapons Research Establishment
Senior Librarian, Weapons Research Establishment
Librarian, R.A.N. Research Laboratory
Scientific & Technical Information Branch
Directorate of Quality Assurance
Principal Librarian, ADSATIS